Environmental Science & Technology

pubs.acs.org/est

Article

# Surface Lattice-Embedded Pt Single-Atom Catalyst on Ceria-Zirconia with Superior Catalytic Performance for Propane Oxidation

Wei Tan, Shaohua Xie, Yandi Cai, Haowei Yu, Kailong Ye, Meiyu Wang, Weijian Diao, Lu Ma, Steven N. Ehrlich, Fei Gao,* Lin Dong, and Fudong Liu*

Cite This: *Environ. Sci. Technol.* 2023, 57, 12501−12512

Read Online

ACCESS | Metrics & More | Article Recommendations | Supporting Information

**ABSTRACT:** Tuning the metal−support interaction and coordination environment of single-atom catalysts can help achieve satisfactory catalytic performance for targeted reactions. Herein, via the facile control of calcination temperatures for Pt catalysts on pre-stabilized $Ce_{0.9}Zr_{0.1}O_2$ (CZO) support, Pt single atoms ($Pt_1$) with different strengths of Pt−$CeO_2$ interaction and coordination environment were successfully constructed. With the increase in calcination temperature from 350 to 750 °C, a stronger Pt−$CeO_2$ interaction and higher Pt-O-Ce coordination number were achieved due to the reaction between $PtO_x$ and surface $Ce^{3+}$ species as well as the migration of $Pt_1$ into the surface lattice of CZO. The Pt/CZO catalyst calcined at 750 °C (Pt/CZO-750) exhibited a surprisingly higher $C_3H_8$ oxidation activity than that calcined at 550 °C (Pt/CZO-550). Through systematic characterizations and reaction mechanism study, it was revealed that the higher concentration of surface $Ce^{3+}$ species/oxygen vacancies and the stronger Pt−$CeO_2$ interaction on Pt/CZO-750 could better facilitate the activation of oxygen to oxidize $C_3H_8$ into reactive carbonate/carboxyl species and further promote the transformation of these intermediates into gaseous $CO_2$. The Pt/CZO-750 catalyst can be a potential candidate for the catalytic removal of hydrocarbons from vehicle exhaust.

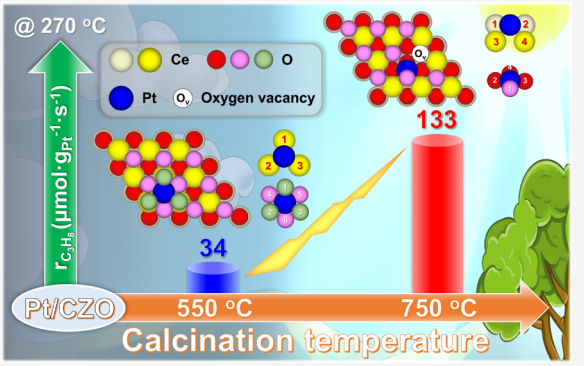


**KEYWORDS:** *Pt single atom, calcination temperature, $C_3H_8$ oxidation reaction, Pt−$CeO_2$ interaction, coordination environment*



## 1. INTRODUCTION

Hydrocarbons (HCs) emitted by vehicles are well known as toxic and detrimental pollutants, which can cause untold damage to both ecological environment and human health by involving in the formation of photochemical smog and haze pollution.[1−3] The most effective way to eliminate HCs from vehicle exhaust such as diesel engine emission is the catalytic complete oxidation of HCs to less harmful $CO_2$ and $H_2O$.[4−7] Unlike CO oxidation, which has been widely studied as an important probe reaction to evaluate the catalytic performance of vehicle emission control catalysts,[8−13] HC oxidation has been given much less attention in environmental catalysis area. This is probably due to the higher difficulty to achieve complete oxidation of HCs to $CO_2$ and $H_2O$ within the required low-temperature range as the short-chain alkanes, main components of HCs emitted by vehicles, are chemically and thermodynamically stable.[14,15]

With the awakening of environmental awareness and the implementation of increasingly stringent vehicle emission regulations, the development of more efficient catalysts for the complete oxidation of short-chain alkanes, especially propane ($C_3H_8$), has become a critical task.[16] So far, the platinum group metals (PGMs), such as Pt, Pd, Ru, *etc.*, supported on refractory metal oxides ($Al_2O_3$, $CeO_2$, $ZrO_2$, *etc.*) are still the most promising candidates for HC oxidation from vehicle exhaust to meet the requirement for excellent low-temperature activity and high (hydro)thermal stability simultaneously.[17−22] To ensure the high catalytic performance of PGM catalysts for HC oxidation, the precise control of PGM dispersion, the development of new supports combined with surface defect engineering, and the fine-tuning of metal−support interaction strength were reported as the most commonly used strategies.[5,15,23−32] For example, Zhan's group systematically studied the impact of spatial distribution of Ru nanoparticles and morphology/exposed facets of $CeO_2$ support on the $C_3H_8$ oxidation performance of Ru/$CeO_2$ catalysts.[15,23] They highlighted that the strong metal−support interaction between Ru and $CeO_2$ could stabilize Ru and also provide active oxygen species for the oxidation of $C_3H_8$ adsorbed on Ru nanoparticles.[24] Fang *et al.* reported that the electronic structure of Pt nanoparticles and chemisorbed

Received: May 8, 2023
Revised: July 28, 2023
Accepted: July 31, 2023
Published: August 11, 2023

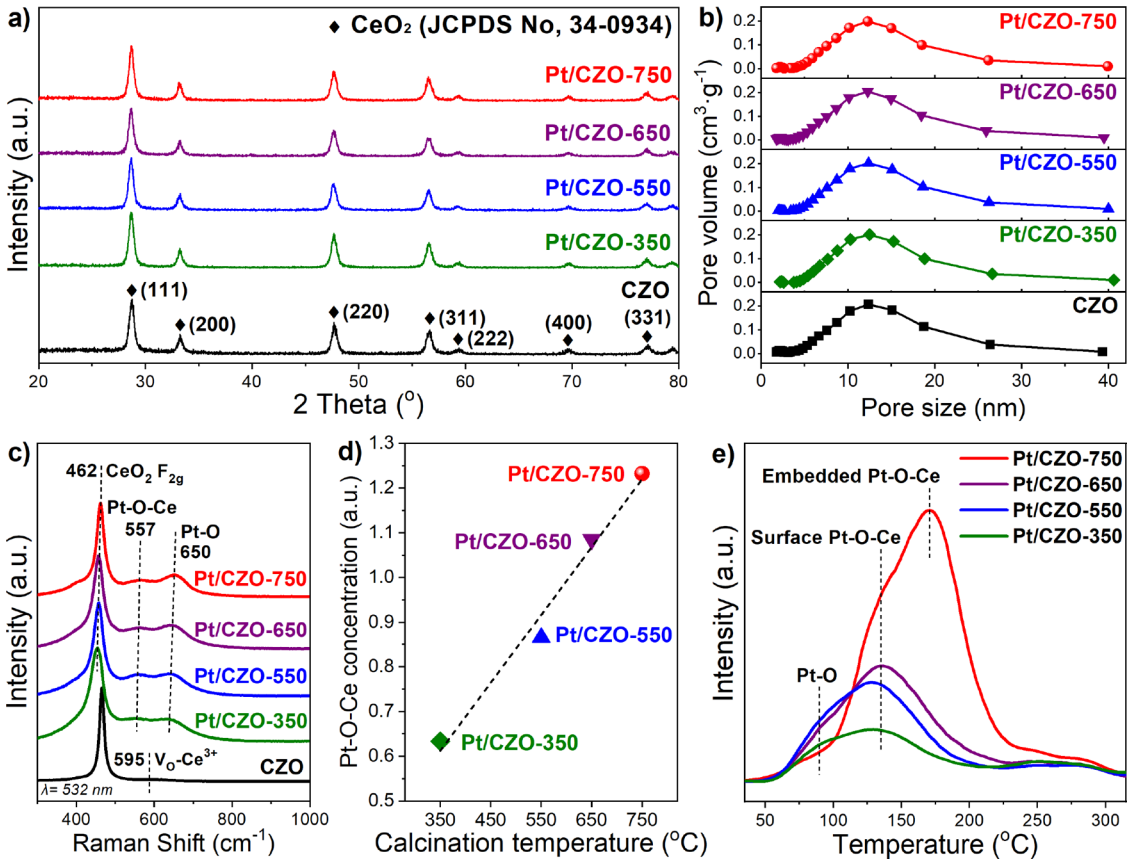


**Figure 1.** (a) XRD patterns, (b) pore size distribution, and (c) Raman spectra for CZO support and Pt/CZO-X catalysts. (d) Relative concentration of the Pt-O-Ce structure on Pt/CZO-*X* catalysts derived from Raman spectra. (e) $H_2$-TPR profiles for Pt/CZO-*X* catalysts (*X* = 350, 550, 650, and 750 °C).

oxygen species on a defective Pt/$TiO_{2-x}$ catalyst determined its catalytic performance in $C_3H_6/C_3H_8$ oxidation.[5] Pt/$Al_2O_3$ and Pd/$Al_2O_3$ catalysts modified with transition metal oxides ($WO_x$, $Nb_2O_5$, $V_2O_5$, *etc.*) were found to exhibit enhanced $C_3H_8$ oxidation activity due to the synergistic effect between Pt/Pd sites and metal oxide promoters.[25−29] The effect of different supports ($TiO_2$, $CeO_2$, $Al_2O_3$, $Nb_2O_5$, *etc.*) for Pt catalysts on HC oxidation performance was also investigated, and it was concluded that the presence of more metallic Pt species and more acidic supports could better facilitate the oxidation of $C_3H_8$.[30,31] With the development of more advanced synthesis and characterization techniques, supported single-atom PGM catalysts have also emerged as a new type of efficient catalytic material for HC oxidation.[33,34]

Recently, Pt single-atom ($Pt_1$) catalysts supported on $CeO_2$-based supports have been intensively studied in CO oxidation due to their near 100% atomic utilization efficiency and satisfactory stability.[35−39] Although the $Pt_1$ catalysts supported on $CeO_2$ are generally considered to show limited CO oxidation activity due to the CO poisoning effect,[40] after fine-tuning the local structure or chemical states of $Pt_1$ species, significantly enhanced CO oxidation performance could be achieved.[36,37,41] For example, Jiang *et al.* found that $Pt_1$ in an asymmetric $Pt_1O_4$ configuration on $CeO_2$ induced by the thermal-shock synthesis method using ultrafast shockwaves in an inert atmosphere (>1200 °C) showed greatly enhanced CO oxidation activity compared to the widely reported $Pt_1/CeO_2$ catalyst prepared by the atom trapping method (800 °C in air).[36] After treatment by $H_2$ at appropriate temperatures (for example, *ca.* 300 °C), the $Pt_1$ species within $Pt_1/CeO_2$-$Al_2O_3$ catalyst with a high $Pt^0$ fraction (above 70%) could also exhibit superior CO oxidation activity at low temperatures.[37] Inspired by these studies, it is hypothesized that the catalytic performance of $Pt_1$ catalysts on $CeO_2$-based supports for $C_3H_8$ oxidation can also be enhanced by controlling the states of $Pt_1$ species, including the Pt−$CeO_2$ interaction strength, oxidation states and coordination environments, *etc.*

Based on our previous work and studies from other researchers, it is inferred that controlling the calcination temperature can be a facile strategy to tune the $Pt_1$ states on $CeO_2$-based supports, during which the atomic-local environment of $Pt_1$ species can evolve remarkably.[42−44] In this study, the $Pt_1$ catalysts with different coordination environments and $Pt_1$−$CeO_2$ interaction strength were constructed on a pre-stabilized $CeO_2$-$ZrO_2$ support by simply controlling the calcination temperatures. The $Pt_1$ species embedded in the $CeO_2$ surface lattice with higher Pt-O-Ce coordination number and stronger Pt−$CeO_2$ interaction could be created as the calcination temperature was set at 750 °C. Although high-temperature calcination or aging usually results in catalyst deactivation, for example, in CO oxidation, the $Pt_1/CeO_2$-$ZrO_2$ catalyst calcined at higher temperature (750 °C) exhibited surprisingly better $C_3H_8$ oxidation performance than that calcined at regular catalyst preparation temperature (such as 550 °C). Through systemic structure characterization and reaction mechanism study, such an unexpectable but beneficial effect of high-temperature calcination on the catalytic performance of $Pt_1$ for $C_3H_8$ oxidation was well


https://doi.org/10.1021/acs.est.3c03497
Environ. Sci. Technol. 2023, 57, 12501−12512

elucidated. This study opens a new route of synthesizing more efficient Pt single-atom catalysts for catalytic removal of $C_3H_8$ in emission control applications.

## 2. MATERIALS AND EXPERIMENTAL METHODS

**2.1. Catalyst Preparation.** Pt catalysts used in this work were supported on a $ZrO_2$-modified $CeO_2$, with a Ce-Zr molar ratio of 9:1 ($Ce_{0.9}Zr_{0.1}O_2$). The $Ce_{0.9}Zr_{0.1}O_2$ support was prepared by the co-precipitation method using $Ce(NO_3)_3 \cdot 6H_2O$ and $ZrO(NO_3)_2$ as precursors. In detail, a calculated amount of $Ce(NO_3)_3 \cdot 6H_2O$ and $ZrO(NO_3)_2$ was first dissolved in deionized water, and then excess $NH_3 \cdot H_2O$ was added under vigorous stirring until the pH reached 10. Afterward, the resulted mixture was aged for 12 h, followed by filtration and washing. The obtained precipitate was dried at 100 °C for 24 h and subsequently calcined at 800 °C for 12 h with a ramping rate of 2 °C·min$^{-1}$. The $Ce_{0.9}Zr_{0.1}O_2$ support was denoted as CZO. 1 wt % Pt (using $Pt(NO_3)_2$ as a precursor) was deposited on CZO support by the conventional incipient wetness impregnation (IWI) method. After drying at 120 °C, the mixture was calcined at 350, 550, 650, or 750 °C for 2 h (with a ramping rate of 5 °C·min$^{-1}$). The obtained Pt/CZO catalysts were denoted as Pt/CZO-*X*, in which -*X* is the calcination temperature in °C.

**2.2. Catalytic Performance Evaluation and Catalyst Characterizations.** The detailed description of catalytic performance evaluation and characterizations in this work can be found in the Supporting Information (Text S1 and Text S2).

## 3. RESULTS AND DISCUSSION

**3.1. Structural Characterization.** Since the Pt catalysts were calcined at different temperatures from 350 to 750 °C after Pt impregnation, the $CeO_2$-based support should be pre-calcined at higher temperatures to minimize its potential structure change during the second calcination. In this work, 800 °C was chosen as the pre-calcination temperature for $CeO_2$-based support. However, after the calcination at 800 °C, the specific surface area of pure $CeO_2$ (prepared by the precipitation method) would decrease significantly, which was detrimental to the formation and stabilization of single atoms. As a result, the $CeO_2$ support used in this work was stabilized by $ZrO_2$ doping (Ce:Zr molar ratio of 9:1) and pre-calcined at 800 °C for 12 h (CZO). As shown in Figure 1a, all peaks in the XRD pattern for CZO could be assigned to $CeO_2$ with a cubic fluorite structure (JCPDS No. 34-0934). Crystalline $ZrO_2$ was not detected by XRD for CZO, indicating that $Zr^{4+}$ was well doped into the $CeO_2$ matrix.[45,46] After the loading of Pt followed by calcination, the peak intensity of cubic fluorite $CeO_2$ within Pt/CZO-350/550/650/750 catalysts almost remained constant, indicating that the CZO support was highly stable during the catalyst fabrication process at different temperatures (350−750 °C). *In situ* XRD experiments under two selected calcination conditions (550 and 750 °C) were also conducted to investigate the crystal structure of Pt/CZO during the calcination process (Figure S1). Besides the observable lattice expansion of $CeO_2$ at elevated temperatures, after cooling down to room temperature, both Pt/CZO-550 and Pt/CZO-750 catalysts showed almost the same XRD patterns as that for uncalcined Pt/CZO, suggesting again the high thermal stability of CZO support. Moreover, in both *ex situ* and *in situ* XRD results, no diffraction peaks assigned to crystalline Pt or $PtO_x$ were observed,[47,48] indicating that the Pt species on CZO support was present in amorphous or highly dispersed state (Figure 1a and Figure S1). The similar type IV isotherms with H1 hysteresis loops for $N_2$ adsorption−desorption (Figure S2) as well as the comparable specific BET surface areas, pore volumes, average pore sizes (Table S1), and pore size distributions (Figure 1b) for CZO support and Pt/CZO-*X* catalysts further supported the viewpoint that the CZO structure was indeed very stable upon the Pt deposition and calcination.

To further reveal the structure of CZO and Pt/CZO-*X*, Raman spectra were collected (Figure 1c). For CZO support, two bands at *ca.* 460 and 595 cm$^{-1}$ showed up, which could be assigned to triply degenerate $F_{2g}$ mode of fluorite-type $CeO_2$ lattice and defect-induced mode due to the existence of oxygen vacancies in $CeO_2$, respectively.[49] After the loading of Pt, a red-shift of the $CeO_2$ $F_{2g}$ band was observed on all Pt/CZO-*X* catalysts, which should result from the larger lattice parameter of $CeO_2$ induced by Pt modification.[49] Moreover, two new bands at *ca.* 557 and 650 cm$^{-1}$ emerged, which were related to the formation of Pt-O-Ce and Pt-O (in Pt-O-Ce) structures, respectively,[40,50] suggesting the strong interaction between Pt and CZO support. The peak area ratio of Pt-O-Ce and Pt-O bands ($I_{\text{Pt-O-Ce + Pt-O}}$) to $CeO_2$ $F_{2g}$ band ($I_{F2g}$), *i.e.*, $I_{\text{Pt-O-Ce + Pt-O}}/I_{F2g}$, was calculated to indicate the relative concentration of Pt-O-Ce structures. As shown in Figure 1d, with the calcination temperature increased, the relative concentration of Pt-O-Ce linkages within Pt/CZO-*X* catalysts showed a monotonic linear increase, suggesting that the high-temperature calcination could drive the Pt species to interact with CZO support more strongly.

$H_2$-TPR is a powerful technique to investigate the redox property and structure of catalytic materials, which was used in this study to further reveal the reducibility and microstructure of Pt/CZO-*X* serial catalysts. As shown in Figure S3, besides the $H_2$-consumption peaks assigned to the reduction of surface $Ce^{4+}$ (300−600 °C) and bulk $CeO_2$ (>600 °C),[51] the $H_2$-consumption peaks at 50−250 °C also showed up on Pt/CZO-*X* serial catalysts, which could be assigned to the reduction of Pt-O and Pt-O-Ce structures as well as $CeO_2$ adjacent to Pt species (Figure 1e, Figure S4, and Table S2).[44,52] When the calcination temperature increased from 350 to 550 °C, a more intensive $H_2$-consumption peak assigned to the surface Pt-O-Ce structure was observed, indicating the dispersion of $PtO_x$ clusters into Pt single atoms. When the calcination temperature further increased from 550 to 750 °C, although the intensity of the $H_2$-consumption peak assigned to the surface Pt-O-Ce structure decreased, a more intensive $H_2$-consumption peak assigned to the embedded Pt-O-Ce structure emerged on Pt/CZO-750, suggesting that a large portion of Pt atoms on Pt/CZO-750 have migrated into the surface lattice of CZO and the formation of more Pt-O-Ce linkages. The shift of the $H_2$-consumption peak assigned to the reduction of the Pt-O-Ce structure to higher temperatures on Pt/CZO catalysts with the increase in calcination temperature suggested the formation of stronger Pt−$CeO_2$ interaction, which was also well supported by the CO-TPR results (Figure S5). Based on characterization results as mentioned above, it can be inferred that the Pt sites with different local coordination structures were successfully created on the highly stable CZO support, which could potentially show distinct catalytic performance. The different colors of Pt/CZO-*X* serial catalysts also hinted at the different states of Pt species on CZO support (Figure S6).



https://doi.org/10.1021/acs.est.3c03497
Environ. Sci. Technol. 2023, 57, 12501−12512

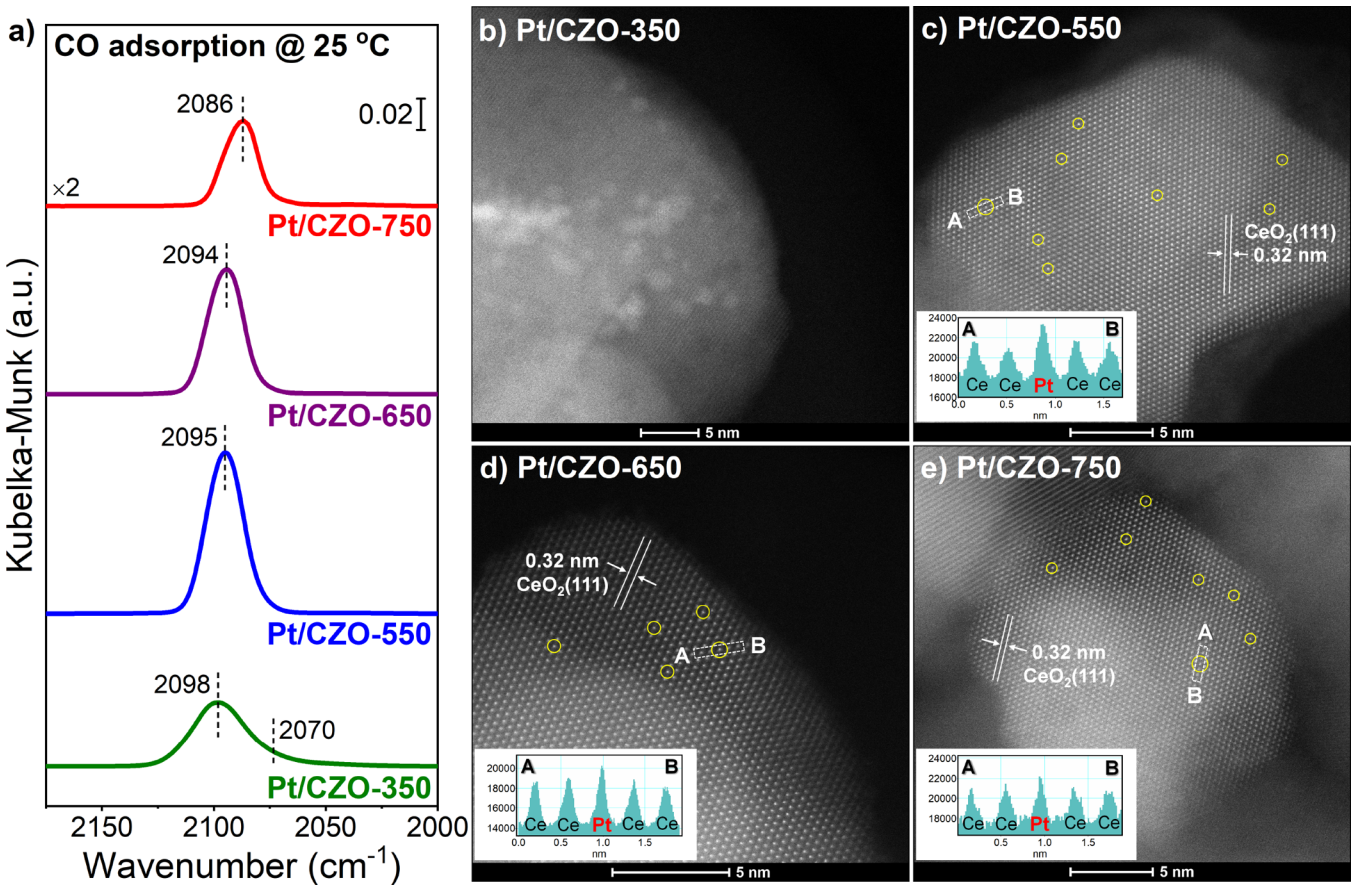


**Figure 2.** (a) *In situ* DRIFTS of CO adsorption at 25 °C on Pt/CZO-*X* catalysts. AC-HAADF-STEM images of (b) Pt/CZO-350, (c) Pt/CZO-550, (d) Pt/CZO-650, and (e) Pt/CZO-750. Note that the inset figures are line profiles to better demonstrate the presence of Pt single atoms, and some line profile signals labeled as Ce atoms might be Zr atoms.

**3.2. Pt Single Atoms on CZO Support.** To further investigate the states of Pt species within Pt/CZO-*X* catalysts, *in situ* DRIFTS of CO adsorption was performed at 25 °C (Figure 2a). On Pt/CZO-350, a dominant band at 2098 $cm^{-1}$ was observed with a shoulder band at *ca.* 2070 $cm^{-1}$ also showing up, which could be assigned to the CO adsorbed on Pt single atoms (CO-$Pt_1$) and CO adsorbed on Pt clusters (CO-Pt cluster), respectively.[53−56] Interestingly, when the calcination temperature was increased to 550 °C or higher, only well-defined symmetric bands at 2095−2086 $cm^{-1}$ could be observed, suggesting that the Pt species on Pt/CZO-550, Pt/CZO-650, and Pt/CZO-750 were mainly in the form of Pt single atoms. The monotonically lowered band intensity with an obvious red-shift in wavenumber as the calcination temperature increased from 550 to 750 °C suggested that the local coordination structure and electronic property of Pt single atoms on CZO might have evolved at elevated temperatures.

AC-HAADF-STEM images of Pt/CZO-*X* serial catalysts were also collected to explore the states of Pt species (Figure 2b−e and Figures S7−S10). Matching well with the *in situ* DRIFTS results of CO adsorption, aggregated Pt species were observed on Pt/CZO-350 (*i.e.*, brighter clusters with an average diameter of *ca.* 2 nm in Figure 2b). On Pt/CZO-550, Pt/CZO-650, and Pt/CZO-750, no clearly identifiable Pt clusters or nanoparticles were present on both on-axis and off-axis AC-HAADF-STEM images (Figure 2c−e and Figures S8−S10). Moreover, the isolated bright dots (marked with yellow circles) were observed and identified as Pt single atoms on the catalysts calcined above 550 °C, which were further verified by the representative line profile results (Figure 2c−e and Figure S11). The enormous difference between the AC-HAADF-STEM images for Pt/CZO-550/650/750 and Pt/CZO-350 also supported that the Pt species on Pt/CZO-*X* should be atomically dispersed when the calcination temperature was higher than 550 °C. Moreover, the Pt single atoms on Pt/CZO-550/650/750 were found to fit well with the Ce column, indicating that Pt single atoms should be located at the different substitution sites or epitaxial growth sites of Ce on CZO support. The EDS mapping results (Figure S12) also showed that both Pt species and Zr species on Pt/CZO-*X* catalysts ($X \geq 550$ °C) were in highly dispersed state without obvious aggregation during high-temperature calcination.

CO oxidation is one of the most prototypical probe reactions to investigate the structure−activity relationship of catalysts in heterogeneous catalysis field.[10] Furthermore, Pt−$CeO_2$-based catalysts have been widely studied for the catalytic oxidation of CO. Therefore, the CO oxidation activity was also evaluated herein to characterize the structural difference of Pt/CZO-*X* serial catalysts. As shown in Figure S13, with the increase in calcination temperature, the CO oxidation activity on Pt/CZO-*X* catalysts showed a monotonic decrease, following Pt/CZO-350 > Pt/CZO-550 > Pt/CZO-650 > Pt/CZO-750. Considering that the bulk structure of CZO support within Pt/CZO-*X* catalysts was almost the same and the Pt species were all in single-atom form for Pt/CZO-550, Pt/


https://doi.org/10.1021/acs.est.3c03497
Environ. Sci. Technol. 2023, 57, 12501−12512

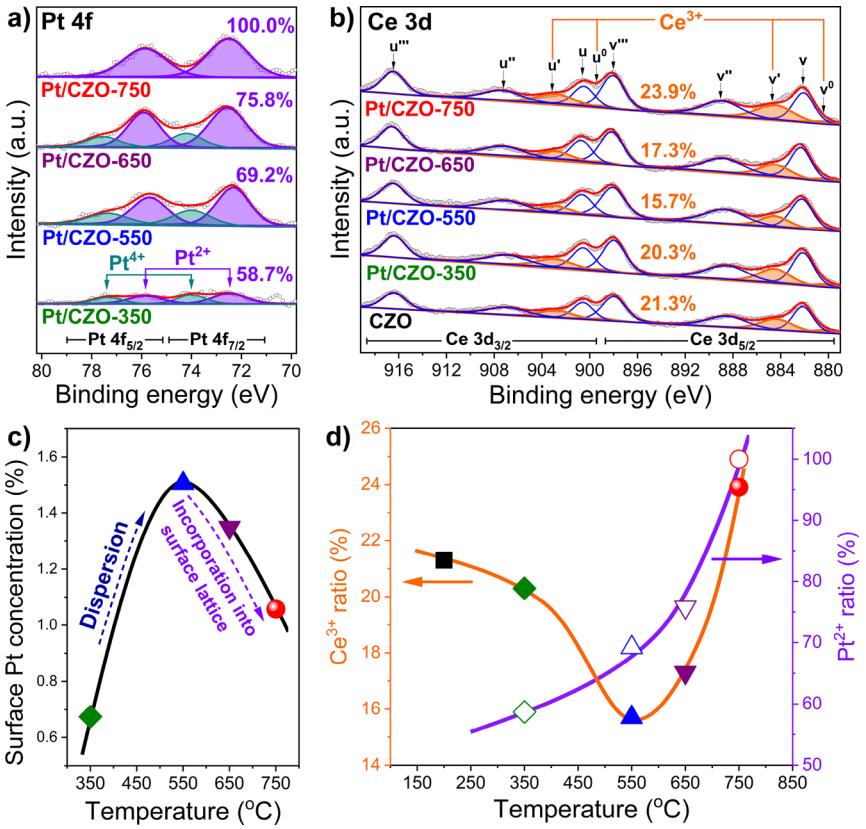


**Figure 3.** (a) Pt 4f XPS for Pt/CZO-*X* serial catalysts; (b) Ce 3d XPS for CZO support and Pt/CZO-*X* catalysts; (c) surface Pt concentration on Pt/CZO-*X* serial catalysts determined by XPS; (d) $Ce^{3+}$ and $Pt^{2+}$ ratios on CZO support and Pt/CZO-*X* catalysts determined by XPS.

CZO-650, and Pt/CZO-750, the strikingly different CO oxidation activities suggested that the $Pt_1$ species on Pt/CZO-*X* catalysts (*X* = 550, 650, and 750) were indeed in different chemical states or located at different sites of CZO support. The similar CO oxidation activity on Pt/CZO-750 to that on CZO support suggested that the Pt atoms on Pt/CZO-750 might have migrated into the surface lattice of CZO.

Based on the results of Raman spectra, $H_2$-TPR, *in situ* DRIFTS of CO adsorption, AC-HAADF-STEM, and CO oxidation activity evaluation, it could be concluded that the elevated calcination temperatures (from 350 to 750 °C) could drive Pt species to disperse on CZO support and facilitate the formation of more Pt-O-Ce linkages as well as stronger Pt−$CeO_2$ interaction. To better elucidate the surface states of Pt/CZO-*X* catalysts, a detailed analysis of XPS results was conducted (Figure 3 and Table S3). As shown in Figure 3a, for Pt 4f XPS, the peaks at *ca.* 72.4 and 75.8 eV were assigned to $Pt^{2+}$ species, while the peaks at *ca.* 74.2 and 77.6 eV were assigned to $Pt^{4+}$ species.[13,40] Accordingly, the Pt species on Pt/CZO-*X* catalysts were all in ionic states. Based on the deconvolution results of Pt 4f XPS, more $Pt^{2+}$ species could be obtained on Pt/CZO catalysts calcined at higher temperatures. For Pt/CZO-750, all Pt species were in $Pt^{2+}$ form, matching well with the previous reports.[35,57] According to the deconvolution results of Ce 3d XPS (Figure 3b and Table S3), the ratio of surface $Ce^{3+}$ species among total Ce species (*i.e.*, $Ce^{3+}/(Ce^{3+} + Ce^{4+})$) first decreased and then increased, with the lowest $Ce^{3+}$ ratio achieved on Pt/CZO-550 (15.7%). For Zr 3d XPS, the peaks at 184.0 and 181.6 eV on CZO could be assigned to $Zr^{4+}$ species,[58] and no shift was observed for these two peaks after Pt deposition and subsequent calcination at different temperatures, suggesting that no significant interaction was formed between Pt and Zr (Figure S14).

The surface concentration of Pt species on Pt/CZO-*X* serial catalysts was also calculated (Table S3 and Figure 3c). When the calcination temperature was increased from 350 to 550 °C, the concentration of Pt species increased significantly from 0.7 to 1.5%, which resulted from the dispersion of Pt clusters to Pt single atoms (Figure 2b−e). When the calcination temperature was further increased to 750 °C, the concentration of Pt species showed an obvious decrease to 1.1%. Since all the Pt species on Pt/CZO-550, Pt/CZO-650, and Pt/CZO-750 were in single-atom form, the lower surface Pt concentration on Pt/CZO-750 than that on Pt/CZO-550 should be due to the migration of Pt single atoms into the surface lattice of CZO at higher calcination temperature, and the Pt single atoms on Pt/CZO-750 should be located at the Ce substitution sites, as suggested by the AC-HAADF-STEM results (Figure 2b−e). The lower intensity of the CO-$Pt_1$ band on Pt/CZO-750 observed in the *in situ* DRIFTS of CO adsorption should also be owing to the Pt migration into the surface lattice of CZO, which significantly reduced the CO adsorption amount (Figure 2a).

The ratios of $Pt^{2+}$ species and $Ce^{3+}$ species on Pt/CZO-*X* serial catalysts were re-organized in Figure 3d to better illustrate the surface structure evolution process under elevated calcination temperatures. After the loading of Pt and subsequent calcination at low temperatures (≤550 °C), the surface $Ce^{3+}$ ratio decreased from 21.3% on CZO to 20.3% on Pt/CZO-350 and then to 15.7% on Pt/CZO-550. Such a decrease in the surface $Ce^{3+}$ ratio could be related to the reaction between $Ce^{3+}$ species and $Pt^{4+}$ species ($PtO_2$), *i.e.*,


https://doi.org/10.1021/acs.est.3c03497
Environ. Sci. Technol. 2023, 57, 12501−12512

$2Ce^{3+} + PtO_2 \rightarrow Ce^{4+}$-O-$Pt^{2+}$-O-$Ce^{4+}$.[57] When the calcination temperature was further increased to 650 and 750 °C, the $Ce^{3+}$ ratio increased to 17.3 and 23.9%, respectively. As concluded above, the Pt single atoms could migrate into the $CeO_2$ surface lattice when calcined at high temperatures (≥650 °C), and the formation of more $Ce^{3+}$ species on Pt/CZO-650 and Pt/CZO-750 could be due to the substitution of $Ce^{4+}$ sites ($r$ = 0.970 Å) by $Pt^{4+}/Pt^{2+}$ with smaller ionic radius ($r$ = 0.625/0.800 Å).[43,59] To balance the surface structure, more $Ce^{3+}$ species ($r$ = 1.143 Å)[60] and $Pt^{2+}$ species with larger ionic radius should be formed on Pt/CZO-$X$ catalysts calcined at higher temperatures (≥650 °C). Moreover, the generation of more surface $Ce^{3+}$ species is always accompanied by the formation of richer oxygen vacancies,[61] which was also the case for Pt/CZO-650 and Pt/CZO-750 catalysts in this study as confirmed by Raman spectra (Figure S15 and Table S3). Based on the results of XPS, Raman spectra, AC-HAADF-STEM, and a previous report,[62] it can be concluded that the calcination temperature, surface mobile oxygen species, and surface defects/$Ce^{3+}$ species could jointly determine the dispersion and location of Pt species on CZO support.

XAS analysis was conducted to further explore the oxidation states and coordination environments of Pt species. As shown in Figure 4a, the white line intensity of Pt-$L_3$ XANES for Pt/CZO-$X$ decreased significantly as the calcination temperature increased, indicating that the Pt species within Pt/CZO-$X$ catalysts calcined at higher temperatures showed lower oxidation states. The further XANES linear fitting results suggested that the average valence states of Pt species within Pt/CZO-$X$ catalysts decreased monotonically from 3.9 ± 0.1 (Pt/CZO-350) to 2.2 ± 0.1 (Pt/CZO-750) (Figure S16 and Table S4), matching well with the trend observed in XPS experiments (Table S3). The decrease in valence states of Pt species after calcination at higher temperatures also well explained the red-shift of CO adsorption IR bands on Pt/CZO-350 to Pt/CZO-750 (Figure 2a). To investigate the local structure of Pt species within Pt/CZO-$X$ catalysts, Pt-$L_3$ EXAFS data were plotted in R space (Figure 4b). For Pt/CZO-350, although the Pt-Pt coordination shell was not observed, the presence of the Pt-O-Pt coordination shell suggested the formation of $PtO_x$ clusters, in agreement with the results of AC-HAADF-STEM and XPS. For Pt/CZO-550, Pt/CZO-650, and Pt/CZO-750, both Pt-O-Pt and Pt-Pt coordination shells were absent, and only Pt-O and Pt-O-Ce coordination shells were observed, further confirming that the Pt species within Pt/CZO-550, Pt/CZO-650, and Pt/CZO-750 were in the form of single atoms. Moreover, according to the curve fitting results of EXAFS (Figure S17 and Table S5), the lower coordination number (CN) of Pt-O was achieved on Pt/CZO-750 ($CN_{Pt-O}$ = 2.5 ± 0.3) compared to that on Pt/CZO-550 ($CN_{Pt-O}$ = 3.6 ± 0.4), suggesting that the Pt single atoms with different coordination environments were constructed within these two catalysts. The lower $CN_{Pt-O}$ on Pt/CZO-$X$ catalysts calcined at higher temperature also well explained their lower valence states. Interestingly, Pt/CZO-750 with lower $CN_{Pt-O}$ actually possessed a higher $CN_{Pt-O-Ce}$ of 2.4 ± 1.2 than Pt/CZO-550 ($CN_{Pt-O-Ce}$ = 2.0 ± 0.2), agreeing well with the results of Raman spectra in which more Pt-O-Ce linkages were formed within Pt/CZO-$X$ catalysts calcined at higher temperatures. This was mainly due to the incorporation of Pt single atoms into the $CeO_2$ surface lattice driven by the high-temperature calcination. In short summary, the local coordination environments of $Pt_1$ on CZO support could be fine-tuned by controlling the calcination temperatures, and $Pt_1$ with low $CN_{Pt-O-Ce}$ and relatively higher $CN_{Pt-O-Ce}$ was successfully created on Pt/CZO-550 and Pt/CZO-750, respectively.

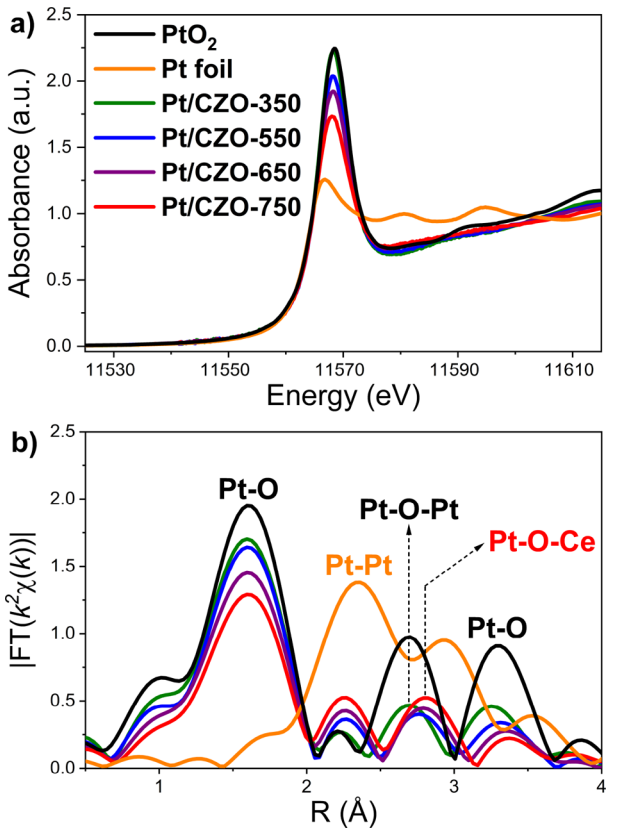


**Figure 4.** (a) Normalized XANES and (b) EXAFS magnitude of the Fourier-transformed $k^2$-weighted $\chi(k)$ data for Pt/CZO-350, Pt/CZO-550, Pt/CZO-650, and Pt/CZO-750 at the Pt-$L_3$ edge. Pt foil and $PtO_2$ were used as references.

**3.3. Catalytic Activity for Propane Oxidation.** Hydrocarbons (HCs) emitted from vehicles powered by different types of engines could result in serious air pollution problems, and the catalytic elimination of short-chain alkanes at low temperatures is still a great challenge in environmental catalysis field. Herein, propane ($C_3H_8$) oxidation was used as a probe reaction to evaluate the potential of Pt/CZO-$X$ catalysts in HC removal for vehicle emission control applications. As shown in Figure 5a and Figure S18, Pt/CZO-550 catalyst showed moderate $C_3H_8$ oxidation activity from 250 to 400 °C, with the $T_{50}$ (the temperature at which $C_3H_8$ conversion reached 50%) observed at 302 °C. Interestingly, the Pt/CZO-750 catalyst showed much higher $C_3H_8$ oxidation activity than Pt/CZO-550, with the $T_{50}$ shifted to 278 °C. The similar $C_3H_8$ oxidation activity on Pt/CZO-750 and Pt/CZO-800 (Pt/CZO catalyst calcined at 800 °C after Pt impregnation) indicated that 750 °C was already a suitable calcination temperature for achieving efficient $C_3H_8$ oxidation activity on Pt/CZO catalyst (Figure S19).

Since there is always abundant $H_2O$ in the vehicle exhaust, which usually also shows a significant impact on the pollutant removal efficiency on particular emission control catalysts, the $C_3H_8$ oxidation activity on Pt/CZO-$X$ catalysts in the presence of $H_2O$ was also tested (Figure 5a and Figure S20). After the introduction of $H_2O$ to the feeding gas, unlike the fact that Pt/


https://doi.org/10.1021/acs.est.3c03497
Environ. Sci. Technol. 2023, 57, 12501−12512

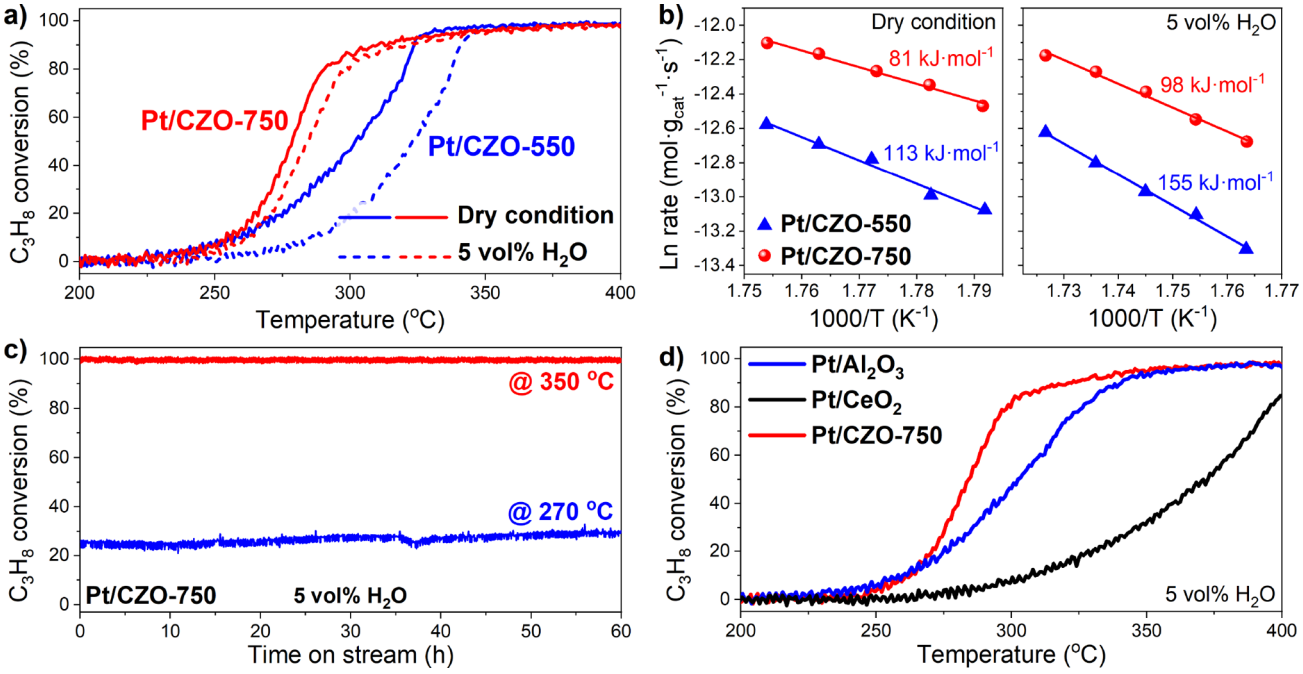


**Figure 5.** (a) $C_3H_8$ oxidation activity on Pt/CZO-550 and Pt/CZO-750 under dry and wet (5 vol % $H_2O$) conditions. (b) Apparent activation energy of $C_3H_8$ oxidation reaction on Pt/CZO-550 and Pt/CZO-750 under dry and wet conditions. (c) $C_3H_8$ oxidation activity on Pt/CZO-750 at 270 and 350 °C in the presence of 5 vol % $H_2O$. (d) $C_3H_8$ oxidation activity on Pt/CZO-750, Pt/$Al_2O_3$, and Pt/$CeO_2$ in the presence of 5 vol % $H_2O$. Reaction condition: 4000 ppm $C_3H_8$, 2% $O_2$, 5 vol % $H_2O$ (when used), Ar as balance, WHSV = 100,000 mL·$g_{cat}^{-1}$·$h^{-1}$.

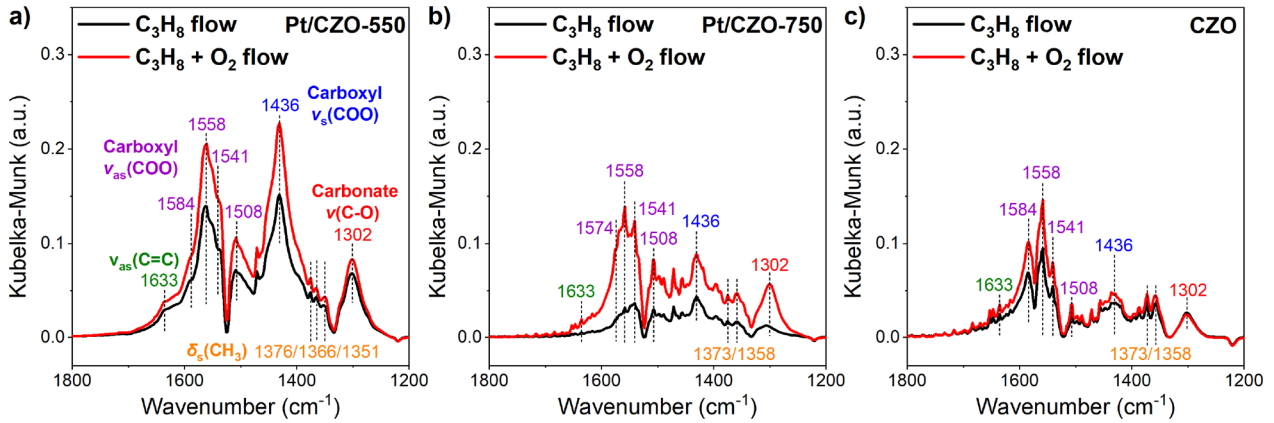


**Figure 6.** *In situ* DRIFTS of $C_3H_8$ adsorption and oxidation on (a) Pt/CZO-550, (b) Pt/CZO-750, and (c) CZO support at 150 °C.

CZO-550 catalyst suffered from severe deactivation, the Pt/CZO-750 catalyst showed much higher resistance to $H_2O$ with the $C_3H_8$ conversion only showing a slight decrease. The much lower apparent activation energy ($E_a$) for $C_3H_8$ oxidation on Pt/CZO-750 under dry and wet conditions (81 and 98 kJ·$mol^{-1}$, respectively) compared to those on Pt/CZO-550 (113 and 155 kJ·$mol^{-1}$, respectively) further supported the viewpoint that Pt/CZO-750 constantly outperformed Pt/CZO-550 in $C_3H_8$ oxidation reaction. As shown in Figure S21, both Pt/CZO-550 and Pt/CZO-750 catalysts exhibited superior $CO_2$ selectivity, suggesting the complete oxidation of $C_3H_8$.

The stability of Pt/CZO-750 under reaction condition was also investigated by a long-term activity test at 270 and 350 °C in the presence of $H_2O$ (Figure 5c). The $C_3H_8$ oxidation activity on Pt/CZO-750 showed no decrease during the test, indicating the superior stability of Pt/CZO-750 under long-term reaction. To further evaluate the stability of Pt/CZO-750, its $SO_2$ and $CO_2$ durability was also evaluated. As shown in Figure S22a, after the introduction of $SO_2$ to the feeding gas, an unexpected enhancement in the $C_3H_8$ oxidation activity was achieved on Pt/CZO-750, which was possibly because the sulfate species formed on Pt/CZO-750 could serve as additional acid sites to facilitate the activation of $C_3H_8$.[30,31] Furthermore, no obvious change was observed in the catalytic performance of Pt/CZO-750 after the addition of 10% $CO_2$, suggesting that $CO_2$ had very limited impact on the $C_3H_8$ oxidation activity on Pt/CZO-750 (Figure S22b). To explore the state of Pt on the most efficient Pt/CZO-750 catalyst after reaction, *in situ* DRIFTS of CO adsorption experiment (25 °C) was conducted on used Pt/CZO-750 (exposed to reaction flow at 300 °C for 1 h). As shown in Figure S23, the position, intensity, and width of the CO adsorption IR band on used Pt/CZO-750 were almost the same as those on fresh Pt/CZO-750, suggesting that the Pt species on used Pt/CZO-750 were still mainly in the form of single atoms. The Pt single atoms on Pt/CZO-750 were highly stable under reaction condition.


https://doi.org/10.1021/acs.est.3c03497
Environ. Sci. Technol. 2023, 57, 12501−12512

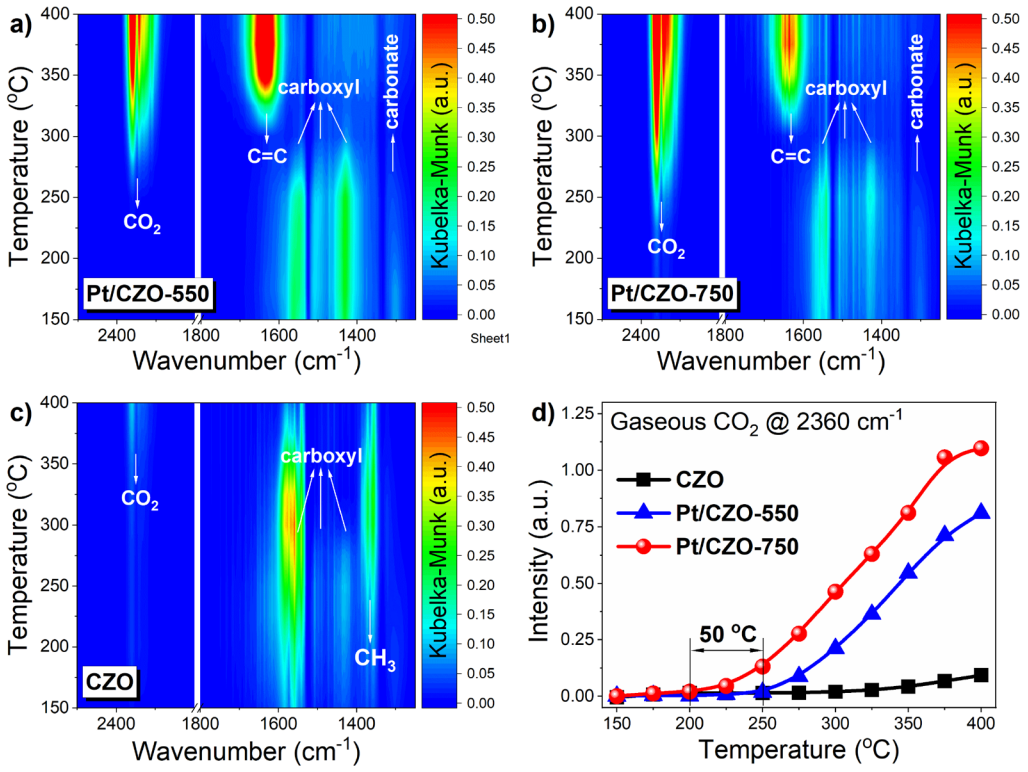


**Figure 7.** *In situ* DRIFTS of $C_3H_8$ oxidation from 150 to 400 °C on (a) Pt/CZO-550, (b) Pt/CZO-750, and (c) CZO. (d) Intensity of the band assigned to gaseous $CO_2$ (at 2360 $cm^{-1}$) during the *in situ* DRIFTS experiments for $C_3H_8$ oxidation.

Besides the superior stability, Pt/CZO-750 also exhibited higher $C_3H_8$ oxidation activity than the conventional Pt catalysts supported on commercial $\gamma$-$Al_2O_3$ and $CeO_2$ (Figure 5d). Compared to the recently reported Pt catalysts for $C_3H_8$ oxidation reaction, Pt/CZO-750 reported herein was still one of the most efficient catalysts (Table S6). The superior catalytic activity, stability, and $CO_2/SO_2$ durability enabled Pt/CZO-750 to be a promising candidate for the efficient catalytic oxidation of $C_3H_8$.

Generally, the calcination or aging treatment at high temperatures (for example, 700 °C or above) usually resulted in the deactivation of catalysts for oxidation reactions. Therefore, it is worth investigating the origin of this unexpected activity promotion for $C_3H_8$ oxidation on Pt/CZO-*X* catalysts induced by high-temperature calcination to establish a clear structure−activity relationship.

**3.4. Reaction Mechanism for Propane Oxidation.** To reveal the intrinsic reason for the higher $C_3H_8$ oxidation activity on Pt/CZO-750 than that on Pt/CZO-550, systematic *in situ* DRIFTS of $C_3H_8$ adsorption and oxidation was performed. As shown in Figure 6, when $C_3H_8$ flow was introduced onto CZO support and Pt/CZO-550 and Pt/CZO-750 catalysts, several bands assigned to carbonate and carboxyl species were observed (1200−1700 $cm^{-1}$).[24,63] The bands at 1302 $cm^{-1}$ could be assigned to $\nu$(C−O) mode in carbonate species.[24,64,65] The bands at 1436 and 1500−1600 $cm^{-1}$ could be attributed to $\nu_s$(COO) and $\nu_{as}$(COO) modes in carboxyl species, respectively.[25,65−67] The bands at 1633 and 1350−1380 $cm^{-1}$ could be assigned to $\nu_{as}$(C═C) and $\delta_s$($CH_3$) modes, respectively.[24,65,68] The formation of oxygenated species indicated that $C_3H_8$ could effectively react with the active oxygen species from CZO support. The bands related to carboxylate and carbonate species on Pt/CZO-750 showed much lower intensity compared to that on Pt/CZO-550, which could result from the fact that the Pt single atoms on Pt/CZO-550 were mainly located at the epitaxial growth sites of Ce on CZO support (fully exposed), while the Pt single atoms on Pt/CZO-750 have migrated into the surface lattice of CZO (partially buried). Interestingly, upon the introduction of $O_2$ into the feed stream, although the bands assigned to carbonate and carboxyl species on Pt/CZO-550 were still more intensive than those on Pt/CZO-750, a more significant enhancement in the intensity of these bands was observed on Pt/CZO-750 than on Pt/CZO-550, suggesting that $O_2$ could be activated more easily on Pt/CZO-750 catalyst to further react with $C_3H_8$ and facilitate the formation of more active intermediate species.[40] As concluded in the sections of Raman spectra and XPS and XAS analysis, more surface defects and oxygen vacancies were formed on Pt/CZO-750 due to the migration of Pt into the surface lattice of CZO and the resulting surface lattice distortion, which should be the main reason for the more efficient $O_2$ activation on Pt/CZO-750. Although ensemble/cluster catalysts have been reported to exhibit higher $C_3H_8$ oxidation activity than single-atom catalysts,[18,69] this work provides new insight into the construction of a Pt single-atom catalyst with superior $C_3H_8$ oxidation activity.

To further monitor the reaction process, *in situ* DRIFTS of $C_3H_8$ oxidation from 150 to 400 °C was conducted, with the temperature ramping rate controlled at 10 °C·$min^{-1}$. As shown in Figure 7a,b, with the increase in the reaction temperature under $C_3H_8$ + $O_2$ flow, the intensity of the bands assigned to carbonate/carboxyl species (1302, 1436, and 1500−1600 $cm^{-1}$) on Pt/CZO-550 and Pt/CZO-750 decreased gradually. Furthermore, as the surface carboxyl/carbonate species decreased, gaseous $CO_2$ at 2300−2400 $cm^{-1}$ was generated accordingly, suggesting that the carbonate/carboxyl species


https://doi.org/10.1021/acs.est.3c03497
Environ. Sci. Technol. 2023, 57, 12501−12512

that resulted from $C_3H_8$ partial oxidation could be important intermediates for the total oxidation of $C_3H_8$ to $CO_2$. In clear contrast, the carboxyl species on CZO support remained stable at as high as 350 °C (Figure 7c), indicating that the Pt single atoms within Pt/CZO-550 and Pt/CZO-750 could effectively promote the further oxidation and decomposition of carbonate/carboxyl species to $CO_2$. On Pt/CZO-750 catalyst, its adsorption capacity for carbonate/carboxyl species was apparently smaller than that on Pt/CZO-550 under different temperatures, suggesting that carbonate/carboxyl species could desorb from Pt/CZO-750 more easily under the reaction condition. As illustrated in Figure 7d, the onset temperature for the generation of gaseous $CO_2$ on Pt/CZO-750 was 50 °C lower than that on Pt/CZO-550, further confirming the easier transformation of adsorbed carbonate/carboxyl species to $CO_2$ at lower temperatures on Pt/CZO-750 catalyst. When the reaction temperature was above 300 °C, new intermediate species containing C═C bonds were clearly observed. However, since high oxidation efficiency of $C_3H_8$ could already be achieved on both Pt/CZO-550 and Pt/CZO-750 above 300 °C (Figure 5), the formation of C═C-containing species should not be the rate-determining step in $C_3H_8$ oxidation reaction on Pt/CZO-*X* catalysts.

## 4. ENVIRONMENTAL IMPLICATIONS

In this work, a facile but effective strategy of tuning the calcination temperature was proposed to optimize the catalytic performance of Pt single atoms supported on $Ce_{0.9}Zr_{0.1}O_2$ (CZO) for $C_3H_8$ oxidation, an important reaction in environmental catalysis field. With the increase in calcination temperature from 350 to 750 °C, Pt species ($PtO_x$) deposited on CZO support first dispersed into Pt single atoms (350 °C → 550 °C) and then migrated into the surface lattice of CZO (550 °C → 750 °C). As a result, the Pt single atoms with stronger Pt−$CeO_2$ interaction, higher $CN_{Pt\text{-}O\text{-}Ce}$, and more $Ce^{3+}$ species and surface oxygen vacancies were achieved on Pt/CZO-750 catalyst. The unique surface structure of Pt/CZO-750 could promote the activation of $O_2$ to further react with $C_3H_8$-forming reactive carbonate/carboxyl and facilitate the further conversion of these intermediate species to gaseous $CO_2$. This work provides a new concept for fine-tuning the surface structure of $Pt_1$−$CeO_2$-based catalysts, achieving high efficiency in hydrocarbon oxidation for emission control applications and benefiting the environmental catalysis community.

## ■ ASSOCIATED CONTENT

### Supporting Information

The Supporting Information is available free of charge at https://pubs.acs.org/doi/10.1021/acs.est.3c03497.

*In situ* XRD, $N_2$ physisorption, XPS, $H_2$-TPR, AC-HAADF-STEM images, EDS mapping results, Raman spectra, CO oxidation activity, $C_3H_8$ oxidation activity under different conditions, *etc.* (DOCX)

## ■ AUTHOR INFORMATION


### Corresponding Authors

**Fei Gao** − *State Key Laboratory of Pollution Control and Resource Reuse, School of Environment; Jiangsu Key Laboratory of Vehicle Emissions Control, Center of Modern Analysis; Key Laboratory of Mesoscopic Chemistry of MOE, School of Chemistry and Chemical Engineering, Nanjing University, Nanjing 210023, China;* orcid.org/0000-0001-8626-5509; Email: gaofei@nju.edu.cn

**Fudong Liu** − *Department of Civil, Environmental, and Construction Engineering, Catalysis Cluster for Renewable Energy and Chemical Transformations (REACT), NanoScience Technology Center (NSTC), University of Central Florida, Orlando, Florida 32816, United States;* orcid.org/0000-0001-8771-5938; Email: fudong.liu@ucf.edu

### Authors

**Wei Tan** − *Department of Civil, Environmental, and Construction Engineering, Catalysis Cluster for Renewable Energy and Chemical Transformations (REACT), NanoScience Technology Center (NSTC), University of Central Florida, Orlando, Florida 32816, United States; State Key Laboratory of Pollution Control and Resource Reuse, School of Environment; Jiangsu Key Laboratory of Vehicle Emissions Control, Center of Modern Analysis; Key Laboratory of Mesoscopic Chemistry of MOE, School of Chemistry and Chemical Engineering, Nanjing University, Nanjing 210023, China;* orcid.org/0000-0002-1481-9346

**Shaohua Xie** − *Department of Civil, Environmental, and Construction Engineering, Catalysis Cluster for Renewable Energy and Chemical Transformations (REACT), NanoScience Technology Center (NSTC), University of Central Florida, Orlando, Florida 32816, United States;* orcid.org/0000-0003-1550-7421

**Yandi Cai** − *State Key Laboratory of Pollution Control and Resource Reuse, School of Environment; Jiangsu Key Laboratory of Vehicle Emissions Control, Center of Modern Analysis; Key Laboratory of Mesoscopic Chemistry of MOE, School of Chemistry and Chemical Engineering, Nanjing University, Nanjing 210023, China*

**Haowei Yu** − *State Key Laboratory of Pollution Control and Resource Reuse, School of Environment; Jiangsu Key Laboratory of Vehicle Emissions Control, Center of Modern Analysis; Key Laboratory of Mesoscopic Chemistry of MOE, School of Chemistry and Chemical Engineering, Nanjing University, Nanjing 210023, China*

**Kailong Ye** − *Department of Civil, Environmental, and Construction Engineering, Catalysis Cluster for Renewable Energy and Chemical Transformations (REACT), NanoScience Technology Center (NSTC), University of Central Florida, Orlando, Florida 32816, United States*

**Meiyu Wang** − *College of Engineering and Applied Sciences, Nanjing University, Nanjing 210093, China*

**Weijian Diao** − *Department of Chemical and Biological Engineering, Villanova University, Villanova, Pennsylvania 19085, United States*

**Lu Ma** − *National Synchrotron Light Source II (NSLS-II), Brookhaven National Laboratory, Upton, New York 11973, United States*

**Steven N. Ehrlich** − *National Synchrotron Light Source II (NSLS-II), Brookhaven National Laboratory, Upton, New York 11973, United States*

**Lin Dong** − *State Key Laboratory of Pollution Control and Resource Reuse, School of Environment; Jiangsu Key Laboratory of Vehicle Emissions Control, Center of Modern Analysis; Key Laboratory of Mesoscopic Chemistry of MOE, School of Chemistry and Chemical Engineering, Nanjing*

*University, Nanjing 210023, China;* orcid.org/0000-0002-8393-6669

Complete contact information is available at: https://pubs.acs.org/10.1021/acs.est.3c03497

### Author Contributions

The manuscript was written through the contributions from all authors. All authors have given approval to the final version of the manuscript.

### Notes

The authors declare no competing financial interest.

## ■ ACKNOWLEDGMENTS

F.L. acknowledges the National Science Foundation grant (CHE-1955343) and Startup Fund from the University of Central Florida (UCF). S.X. thanks the support from the Preeminent Postdoctoral Program (P3) at UCF. F.L. sincerely thanks Mr. Hiroshi Kodama and Mr. Sho Hasegawa at Daiichi Kigenso Kagaku Kogyo Co., Ltd., for providing raw materials in catalyst synthesis. L.D. thanks the support from the National Natural Science Foundation of China (No. 22272077). F.G. acknowledges the support from the National Natural Science Foundation of China (No. 21972063) and Natural Science Foundation of Jiangsu Province (BK20200012). This research used beamline 7-BM (QAS) of the National Synchrotron Light Source II, a U.S. Department of Energy (DOE) Office of Science User Facility operated for the DOE Office of Science by Brookhaven National Laboratory under Contract No. DE-SC0012704.

## ■ REFERENCES

(1) Twigg, M. V. Progress and Future Challenges in Controlling Automotive Exhaust Gas Emissions. *Appl. Catal., B* **2007**, *70*, 2−15.
(2) Reşitoğlu, İ. A.; Altinişik, K.; Keskin, A. The Pollutant Emissions from Diesel-Engine Vehicles and Exhaust Aftertreatment Systems. *Clean Technol. Environ. Policy* **2015**, *17*, 15−27.
(3) Chang, D.; Wang, Z.; Guo, J.; Li, T.; Liang, Y.; Kang, L.; Xia, M.; Wang, Y.; Yu, C.; Yun, H.; Yue, D.; Wang, T. Characterization of Organic Aerosols and their Precursors in Southern China during a Severe Haze Episode in January 2017. *Sci. Total Environ.* **2019**, *691*, 101−111.
(4) Datye, A. K.; Votsmeier, M. Opportunities and Challenges in the Development of Advanced Materials for Emission Control Catalysts. *Nat. Mater.* **2021**, *20*, 1049−1059.
(5) Fang, Y.; Li, H.; Zhang, Q.; Wang, C.; Xu, J.; Shen, H.; Yang, J.; Pan, C.; Zhu, Y.; Luo, Z.; Guo, Y. Oxygen Vacancy-Governed Opposite Catalytic Performance for $C_3H_6$ and $C_3H_8$ Combustion: The Effect of the Pt Electronic Structure and Chemisorbed Oxygen Species. *Environ. Sci. Technol.* **2022**, *56*, 3245−3257.
(6) Fang, Y.; Li, L.; Yang, J.; Hoang, S.; Wang, L.; Xu, J.; Yang, W.; Pan, C.; Zhu, Y.; Deng, H.; Luo, Z.; Sun, C.; Gao, D.; Li, Z.; Guo, Y. Engineering the Nucleophilic Active Oxygen Species in $CuTiO_x$ for Efficient Low-Temperature Propene Combustion. *Environ. Sci. Technol.* **2020**, *54*, 15476−15488.
(7) Hu, Z.; Qiu, S.; You, Y.; Guo, Y.; Guo, Y.; Wang, L.; Zhan, W.; Lu, G. Hydrothermal Synthesis of $NiCeO_x$ Nanosheets and its Application to the Total Oxidation of Propane. *Appl. Catal., B* **2018**, *225*, 110−120.
(8) Beniya, A.; Higashi, S. Towards Dense Single-Atom Catalysts for Future Automotive Applications. *Nat. Catal.* **2019**, *2*, 590−602.
(9) Bunluesin, T.; Gorte, R. J.; Graham, G. W. CO Oxidation for the Characterization of Reducibility in Oxygen Storage Components of Three-Way Automotive Catalysts. *Appl. Catal., B* **1997**, *14*, 105−115.
(10) Freund, H.-J.; Meijer, G.; Scheffler, M.; Schlögl, R.; Wolf, M. CO Oxidation as a Prototypical Reaction for Heterogeneous Processes. *Angew. Chem., Int. Ed.* **2011**, *50*, 10064−10094.
(11) Therrien, A. J.; Hensley, A. J. R.; Marcinkowski, M. D.; Zhang, R.; Lucci, F. R.; Coughlin, B.; Schilling, A. C.; McEwen, J.-S.; Sykes, E. C. H. An Atomic-Scale View of Single-Site Pt Catalysis for Low-Temperature CO Oxidation. *Nat. Catal.* **2018**, *1*, 192−198.
(12) Liu, J.; Liu, B.; Fang, Y.; Zhao, Z.; Wei, Y.; Gong, X.-Q.; Xu, C.; Duan, A.; Jiang, G. Preparation, Characterization and Origin of Highly Active and Thermally Stable Pd-$Ce_{0.8}Zr_{0.2}O_2$ Catalysts via Sol-Evaporation Induced Self-Assembly Method. *Environ. Sci. Technol.* **2014**, *48*, 12403−12410.
(13) Zhang, J.; Qin, X.; Chu, X.; Chen, M.; Chen, X.; Chen, J.; He, H.; Zhang, C. Tuning Metal-Support Interaction of Pt-$CeO_2$ Catalysts for Enhanced Oxidation Reactivity. *Environ. Sci. Technol.* **2021**, *55*, 16687−16698.
(14) Labinger, J. A.; Bercaw, J. E. Understanding and Exploiting C-H Bond Activation. *Nature* **2002**, *417*, 507−514.
(15) Zheng, W.; Huang, Z.; Brosnahan, J. T.; Zhang, S.; Guo, Y.; Guo, Y.; Wang, L.; Wang, Y.; Zhan, W. Ru/$CeO_2$ Catalyst with Optimized $CeO_2$ Support Morphology and Surface Facets for Propane Combustion. *Environ. Sci. Technol.* **2019**, *53*, 5349−5358.
(16) Kamal, M. S.; Razzak, S. A.; Hossain, M. M. Catalytic Oxidation of Volatile Organic Compounds (VOCs) - A Review. *Atmos. Environ.* **2016**, *140*, 117−134.
(17) Xie, S.; Wang, Z.; Tan, W.; Zhu, Y.; Collier, S.; Ma, L.; Ehrlich, S. N.; Xu, P.; Yan, Y.; Xu, T.; Deng, J.; Liu, F. Highly Active and Stable Palladium Catalysts on Novel Ceria-Alumina Supports for Efficient Oxidation of Carbon Monoxide and Hydrocarbons. *Environ. Sci. Technol.* **2021**, *55*, 7624−7633.
(18) Jeong, H.; Kwon, O.; Kim, B.-S.; Bae, J.; Shin, S.; Kim, H.-E.; Kim, J.; Lee, H. Highly Durable Metal Ensemble Catalysts with Full Dispersion for Automotive Applications Beyond Single-Atom Catalysts. *Nat. Catal.* **2020**, *3*, 368−375.
(19) Xiong, H.; Wiebenga, M. H.; Carrillo, C.; Gaudet, J. R.; Pham, H. N.; Kunwar, D.; Oh, S. H.; Qi, G.; Kim, C. H.; Datye, A. K. Design Considerations for Low-Temperature Hydrocarbon Oxidation Reactions on Pd Based Catalysts. *Appl. Catal., B* **2018**, *236*, 436−444.
(20) Tan, W.; Alsenani, H.; Xie, S.; Cai, Y.; Xu, P.; Liu, A.; Ji, J.; Gao, F.; Dong, L.; Chukwu, E.; Yang, M.; Liu, F. Tuning Single-atom $Pt_1$-$CeO_2$ Catalyst for Efficient CO and $C_3H_6$ Oxidation: Size Effect of Ceria on Pt Structural Evolution. *ChemNanoMat* **2020**, *6*, 1797−1805.
(21) Wang, Z.; Wang, W.; Khalid, O.; Weber, T.; Spriewald Luciano, A.; Zhan, W.; Smarsly, B. M.; Over, H. Supported $Ru_xIr_{1-x}O_2$ Mixed Oxides Catalysts for Propane Combustion: Resistance Against Water Poisoning. *ChemCatChem* **2022**, *14*, No. e202200149.
(22) Cen, B.; Tang, C.; Lu, J.; Chen, J.; Luo, M. Different Roles of $MoO_3$ and $Nb_2O_5$ Promotion in Short-Chain Alkane Combustion over Pt/$ZrO_2$ Catalysts. *Chin. J. Catal.* **2021**, *42*, 2287−2295.
(23) Sun, Y.; Ye, F.; Ding, J.; Li, J.; Guo, Y.; Wang, L.; Guo, Y.; Dai, S.; Zhan, W. Regulating the Spatial Distribution of Ru Nanoparticles on $CeO_2$ Support for Enhanced Propane Oxidation. *ACS Appl. Nano Mater.* **2022**, *5*, 3937−3945.
(24) Hu, Z.; Wang, Z.; Guo, Y.; Wang, L.; Guo, Y.; Zhang, J.; Zhan, W. Total Oxidation of Propane over a Ru/$CeO_2$ Catalyst at Low Temperature. *Environ. Sci. Technol.* **2018**, *52*, 9531−9541.
(25) Wu, X.; Zhang, L.; Weng, D.; Liu, S.; Si, Z.; Fan, J. Total Oxidation of Propane on Pt/$WO_x$/$Al_2O_3$ Catalysts by Formation of Metastable $Pt^{\delta+}$ Species Interacted with $WO_x$ Clusters. *J. Hazard. Mater.* **2012**, *225-226*, 146−154.
(26) Garcia, T.; Agouram, S.; Taylor, S. H.; Morgan, D.; Dejoz, A.; Vázquez, I.; Solsona, B. Total Oxidation of Propane in Vanadia-Promoted Platinum-Alumina Catalysts: Influence of the Order of Impregnation. *Catal. Today* **2015**, *254*, 12−20.
(27) Zhao, P.; Li, X.; Liao, W.; Wang, Y.; Chen, J.; Lu, J.; Luo, M. Understanding the Role of $NbO_x$ on Pt/$Al_2O_3$ for Effective Catalytic Propane Oxidation. *Ind. Eng. Chem. Res.* **2019**, *58*, 21945−21952.

(28) Noronha, F. B.; Aranda, D. A. G.; Ordine, A. P.; Schmal, M. The Promoting Effect of $Nb_2O_5$ Addition to $Pd/Al_2O_3$ Catalysts on Propane Oxidation. *Catal. Today* **2000**, *57*, 275−282.
(29) Garcia, T.; Weng, W.; Solsona, B.; Carter, E.; Carley, A. F.; Kiely, C. J.; Taylor, S. H. The Significance of the Order of Impregnation on the Activity of Vanadia Promoted Palladium-Alumina Catalysts for Propane Total Oxidation. *Catal. Sci. Technol.* **2011**, *1*, 1367−1375.
(30) Avila, M. S.; Vignatti, C. I.; Apesteguía, C. R.; Garetto, T. F. Effect of Support on the Deep Oxidation of Propane and Propylene on Pt-Based Catalysts. *Chem. Eng. J.* **2014**, *241*, 52−59.
(31) Yoshida, H.; Yazawa, Y.; Hattori, T. Effects of Support and Additive on Oxidation State and Activity of Pt Catalyst in Propane Combustion. *Catal. Today* **2003**, *87*, 19−28.
(32) Wang, F.; He, G.; Zhang, B.; Chen, M.; Chen, X.; Zhang, C.; He, H. Insights into the Activation Effect of $H_2$ Pretreatment on $Ag/Al_2O_3$ Catalyst for the Selective Oxidation of Ammonia. *ACS Catal.* **2019**, *9*, 1437−1445.
(33) Hoang, S.; Guo, Y.; Binder, A. J.; Tang, W.; Wang, S.; Liu, J.; Tran, H.; Lu, X.; Wang, Y.; Ding, Y.; Kyriakidou, E. A.; Yang, J.; Toops, T. J.; Pauly, T. R.; Ramprasad, R.; Gao, P.-X. Activating Low-Temperature Diesel Oxidation by Single-Atom Pt on $TiO_2$ Nanowire Array. *Nat. Commun.* **2020**, *11*, 1062.
(34) Zhang, L.; Xue, L.; Lin, B.; Zhao, Q.; Wan, S.; Wang, Y.; Jia, H.; Xiong, H. Noble Metal Single-Atom Catalysts for the Catalytic Oxidation of Volatile Organic Compounds. *ChemSusChem* **2022**, *15*, No. e202102494.
(35) Nie, L.; Mei, D.; Xiong, H.; Peng, B.; Ren, Z.; Hernandez, X. I. P.; DeLaRiva, A.; Wang, M.; Engelhard, M. H.; Kovarik, L.; Datye, A. K.; Wang, Y. Activation of Surface Lattice Oxygen in Single-Atom $Pt/CeO_2$ for Low-Temperature CO Oxidation. *Science* **2017**, *358*, 1419−1423.
(36) Jiang, D.; Yao, Y.; Li, T.; Wan, G.; Pereira-Hernández, X. I.; Lu, Y.; Tian, J.; Khivantsev, K.; Engelhard, M. H.; Sun, C.; García-Vargas, C. E.; Hoffman, A. S.; Bare, S. R.; Datye, A. K.; Hu, L.; Wang, Y. Tailoring the Local Environment of Platinum in Single-Atom $Pt_1/CeO_2$ Catalysts for Robust Low-Temperature CO Oxidation. *Angew. Chem., Int. Ed.* **2021**, *133*, 26258−26266.
(37) Jeong, H.; Shin, D.; Kim, B.-S.; Bae, J.; Shin, S.; Choe, C.; Han, J. W.; Lee, H. Controlling the Oxidation State of Pt Single Atoms for Maximizing Catalytic Activity. *Angew. Chem., Int. Ed.* **2020**, *59*, 20872−20877.
(38) Ye, X.; Wang, H.; Lin, Y.; Liu, X.; Cao, L.; Gu, J.; Lu, J. Insight of the Stability and Activity of Platinum Single Atoms on Ceria. *Nano Res.* **2019**, *12*, 1401−1409.
(39) Wang, C.; Gu, X. K.; Yan, H.; Lin, Y.; Li, J.; Liu, D.; Li, W.-X.; Lu, J. Water-Mediated Mars-Van Krevelen Mechanism for CO Oxidation on Ceria-Supported Single-Atom $Pt_1$ Catalyst. *ACS Catal.* **2017**, *7*, 887−891.
(40) Pereira-Hernández, X. I.; DeLaRiva, A.; Muravev, V.; Kunwar, D.; Xiong, H.; Sudduth, B.; Engelhard, M.; Kovarik, L.; Hensen, E. J. M.; Wang, Y.; Datye, A. K. Tuning Pt-$CeO_2$ Interactions by High-Temperature Vapor-Phase Synthesis for Improved Reducibility of Lattice Oxygen. *Nat. Commun.* **2019**, *10*, 1358.
(41) Liu, J.-X.; Su, Y.; Filot, I. A. W.; Hensen, E. J. M. Linear Scaling Relation for CO Oxidation on $CeO_2$-Supported Pd. *J. Am. Chem. Soc.* **2018**, *140*, 4580−4587.
(42) Tan, W.; Xie, S.; Cai, Y.; Wang, M.; Yu, S.; Low, K.-B.; Li, Y.; Ma; Ehrlich, S. N.; Gao, F.; Dong, L.; Liu, F. Transformation of Highly Stable Pt Single Sites on Defect Engineered Ceria into Robust Pt Clusters for Vehicle Emission Control. *Environ. Sci. Technol.* **2021**, *55*, 12607−12618.
(43) Bugrova, T. A.; Kharlamova, T. S.; Svetlichnyi, V. A.; Savel'eva, A. S.; Salaev, M. A.; Mamontov, G. V. Insights into Formation of Pt Species in $Pt/CeO_2$ Catalysts: Effect of Treatment Conditions and Metal-Support Interaction. *Catal. Today* **2021**, *375*, 36−47.
(44) Lee, J.; Ryou, Y.; Chan, X.; Kim, T. J.; Kim, D. H. How Pt Interacts with $CeO_2$ under the Reducing and Oxidizing Environments at Elevated Temperature: The Origin of Improved Thermal Stability of $Pt/CeO_2$ Compared to $CeO_2$. *J. Phys. Chem. C* **2016**, *120*, 25870−25879.
(45) Liu, L.; Yao, Z.; Liu, B.; Dong, L. Correlation of Structural Characteristics with Catalytic Performance of $CuO/Ce_xZr_{1-x}O_2$ Catalysts for NO Reduction by CO. *J. Catal.* **2010**, *275*, 45−60.
(46) Tan, W.; Wang, J.; Li, L.; Liu, A.; Song, G.; Guo, K.; Luo, Y.; Liu, F.; Gao, F.; Dong, L. Gas Phase Sulfation of Ceria-Zirconia Solid Solutions for Generating Highly Efficient and $SO_2$ Resistant $NH_3$-SCR Catalysts for NO Removal. *J. Hazard. Mater.* **2020**, *388*, No. 121729.
(47) Gao, M.-R.; Lin, Z.-Y.; Jiang, J.; Cui, C.-H.; Zheng, Y.-R.; Yu, S.-H. Completely Green Synthesis of Colloid Adams' Catalyst $\alpha$-$PtO_2$ Nanocrystals and Derivative Pt Nanocrystals with High Activity and Stability for Oxygen Reduction. *Chem. − Eur. J.* **2012**, *18*, 8423−8429.
(48) Bera, P.; Priolkar, K. R.; Gayen, A.; Sarode, P. R.; Hegde, M. S.; Emura, S.; Kumashiro, R.; Jayaram, V.; Subbanna, G. N. Ionic Dispersion of Pt over $CeO_2$ by the Combustion Method: Structural Investigation by XRD, TEM, XPS, and EXAFS. *Chem. Mater.* **2003**, *15*, 2049−2060.
(49) Loridant, S. Raman Spectroscopy as a Powerful Tool to Characterize Ceria-Based Catalysts. *Catal. Today* **2021**, *373*, 98−111.
(50) Brogan, M. S.; Dines, T. J.; Cairns, J. A. Raman Spectroscopic Study of the Pt-$CeO_2$ Interaction in the $Pt/Al_2O_3$-$CeO_2$ Catalyst. *J. Chem. Soc., Faraday Trans.* **1994**, *90*, 1461−1466.
(51) Ma, Z.; Zhao, S.; Pei, X.; Xiong, X.; Hu, B. New Insights into the Support Morphology-Dependent Ammonia Synthesis Activity of $Ru/CeO_2$ Catalysts. *Catal. Sci. Technol.* **2017**, *7*, 191−199.
(52) Gao, Y.; Wang, W.; Chang, S.; Huang, W. Morphology Effect of $CeO_2$ Support in the Preparation, Metal-Support Interaction, and Catalytic Performance of $Pt/CeO_2$ Catalysts. *ChemCatChem* **2013**, *5*, 3610−3620.
(53) Li, J.; Guan, Q.; Wu, H.; Liu, W.; Lin, Y.; Sun, Z.; Ye, X.; Zheng, X.; Pan, H.; Zhu, J.; Chen, S.; Zhang, W.; Wei, S.; Lu, J. Highly Active and Stable Metal Single-Atom Catalysts Achieved by Strong Electronic Metal-Support Interactions. *J. Am. Chem. Soc.* **2019**, *141*, 14515−14519.
(54) Fan, L.; Wang, K.; Xu, K.; Liang, Z.; Wang, H.; Zhou, S.-F.; Zhan, G. Structural Isomerism of Two Ce-BTC for Fabricating $Pt/CeO_2$ Nanorods toward Low-Temperature CO Oxidation. *Small* **2020**, *16*, 2003597.
(55) Avanesian, T.; Dai, S.; Kale, M. J.; Graham, G. W.; Pan, X.; Christopher, P. Quantitative and Atomic-Scale View of CO-Induced Pt Nanoparticle Surface Reconstruction at Saturation Coverage via DFT Calculations Coupled with *in Situ* TEM and IR. *J. Am. Chem. Soc.* **2017**, *139*, 4551−4558.
(56) Ding, K.; Gulec, A.; Johnson, A. M.; Schweitzer, N. M.; Stucky, G. D.; Marks, L. D.; Stair, P. C. Identification of Active Sites in CO Oxidation and Water-Gas Shift over Supported Pt Catalysts. *Science* **2015**, *350*, 189−192.
(57) Kunwar, D.; Zhou, S.; DeLaRiva, A.; Peterson, E. J.; Xiong, H.; Pereira-Hernández, X. I.; Purdy, S. C.; ter Veen, R.; Brongersma, H. H.; Miller, J. T.; Hashiguchi, H.; Kovarik, L.; Lin, S.; Guo, H.; Wang, Y.; Datye, A. K. Stabilizing High Metal Loadings of Thermally Stable Platinum Single Atoms on an Industrial Catalyst Support. *ACS Catal.* **2019**, *9*, 3978−3990.
(58) Kumar, S.; Kumar, S.; Tiwari, S.; Srivastava, S.; Srivastava, M.; Yadav, B. K.; Kumar, S.; Tran, T. T.; Dewan, A. K.; Mulchandani, A.; Sharma, J. G.; Maji, S.; Malhotra, B. D. Biofunctionalized Nanostructured Zirconia for Biomedical Application: A Smart Approach for Oral Cancer Detection. *Adv. Sci.* **2015**, *2*, 1500048.
(59) Mukri, B. D.; Waghmare, U. V.; Hegde, M. S. Platinum Ion-Doped $TiO_2$: High Catalytic Activity of $Pt^{2+}$ with Oxide Ion Vacancy in $Ti^{4+}_{1-x}Pt^{2+}_xO_{2-x}$ Compared to $Pt^{4+}$ without Oxide Ion Vacancy in $Ti^{4+}_{1-x}Pt^{2+}_xO_2$. *Chem. Mater.* **2013**, *25*, 3822−3833.
(60) Lee, Y.; He, G.; Akey, A. J.; Si, R.; Flytzani-Stephanopoulos, M.; Herman, I. P. Raman Analysis of Mode Softening in Nanoparticle $CeO_{2-\delta}$ and Au-$CeO_{2-\delta}$ during CO Oxidation. *J. Am. Chem. Soc.* **2011**, *133*, 12952−12955.

(61) Borges, L. R.; da Silva, A. G. M.; Braga, A. H.; Rossi, L. M.; Suller Garcia, M. A.; Vidinha, P. Towards the Effect of $Pt^0/Pt^{\delta+}$ and $Ce^{3+}$ Species at the Surface of $CeO_2$ Crystals: Understanding the Nature of the Interactions under CO Oxidation Conditions. *ChemCatChem* **2021**, *13*, 1340−1354.
(62) Nagai, Y.; Hirabayashi, T.; Dohmae, K.; Takagi, N.; Minami, T.; Shinjoh, H.; Matsumoto, S. I. Sintering inhibition mechanism of platinum supported on ceria-based oxide and Pt-oxide−support interaction. *J. Catal.* **2006**, *242*, 103−109.
(63) Lu, Y.; Wang, J.; Yu, L.; Kovarik, L.; Zhang, X.; Hoffman, A. S.; Gallo, A.; Bare, S. R.; Sokaras, D.; Kroll, T.; Dagle, V.; Xin, H.; Karim, A. M. Identification of the Active Complex for CO Oxidation over Single-Atom Ir-on-$MgAl_2O_4$ Catalysts. *Nat. Catal.* **2019**, *2*, 149−156.
(64) Rachmady, W.; Vannice, M. A. Acetic Acid Reduction to Acetaldehyde over Iron Catalysts: II. Characterization by Mössbauer Spectroscopy, DRIFTS, TPD, and TPR. *J. Catal.* **2002**, *208*, 170−179.
(65) Chen, L.; Zhu, Y.; Zheng, H.; Zhang, C.; Li, Y. Aqueous-Phase Hydrodeoxygenation of Propanoic Acid over the $Ru/ZrO_2$ and Ru-Mo/$ZrO_2$ Catalysts. *Appl. Catal., A* **2012**, *411-412*, 95−104.
(66) Swislocki, S.; Stöwe, K.; Maier, W. F. Catalysts for Selective Propane Oxidation in the Presence of Carbon Monoxide: Mechanistic Aspects. *J. Catal.* **2014**, *316*, 219−230.
(67) O'Brien, C. P.; Lee, I. C. A Detailed Spectroscopic Analysis of the Growth of Oxy-Carbon Species on the Surface of $Pt/Al_2O_3$ During Propane Oxidation. *J. Catal.* **2017**, *347*, 1−8.
(68) Hoost, T. E.; Laframboise, K. A.; Otto, K. Co-Adsorption of Propene and Nitrogen Oxides on Cu-ZSM-5: An FTIR Study. *Appl. Catal., B* **1995**, *7*, 79−93.
(69) Jeong, H.; Lee, G.; Kim, B.-S.; Bae, J.; Han, J. W.; Lee, H. Fully Dispersed Rh Ensemble Catalyst To Enhance Low-Temperature Activity. *J. Am. Chem. Soc.* **2018**, *140*, 9558−9565.


https://doi.org/10.1021/acs.est.3c03497
*Environ. Sci. Technol.* 2023, 57, 12501−12512